Published in final edited form as:
Dev Biol. 2010 March 1; 339(1): 126–140. doi:10.1016/j.ydbio.2009.12.021.

Kinesin-dependent transport results in polarized migration of the nucleus in oocytes and inward movement of yolk granules in meiotic embryos

Karen L. McNally[1,3], **Judy L. Martin**[1,3], **Marina Ellefson**[1], and **Francis J. McNally**[1,2]
[1] Section of Molecular and Cellular Biology, 149 Briggs Hall, University of California, Davis, Davis, CA 95616, USA

Abstract

During female meiosis, meiotic spindles are positioned at the oocyte cortex to allow expulsion of chromosomes into polar bodies. In *C. elegans*, kinesin-dependent translocation of the entire spindle to the cortex precedes dynein-dependent rotation of one spindle pole toward the cortex. To elucidate the role of kinesin-1 in spindle translocation, we examined the localization of kinesin subunits in meiotic embryos. Surprisingly, kinesin-1 was not associated with the spindle and instead was restricted to the cytoplasm in the middle of the embryo. Yolk granules moved on linear tracks, in a kinesin-dependent manner, away from the cortex, resulting in their concentration in the middle of the embryo where the kinesin was concentrated. These results suggest that cytoplasmic microtubules might be arranged with plus ends extending inward, away from the cortex. This microtubule arrangement would not be consistent with direct transport of the meiotic spindle toward the cortex by kinesin-1. In maturing oocytes, the nucleus underwent kinesin-dependent migration to the future site of spindle attachment at the anterior cortex. Thus the spindle translocation defect observed in kinesin-1 mutants may be a result of failed nuclear migration, which places the spindle too far from the cortex for the spindle translocation mechanism to function.

INTRODUCTION

Female meiosis in all animals is mediated by meiotic spindles that are attached to the egg cortex by one pole during anaphase. In many species, this cortical spindle attachment allows expulsion of half the homologous chromosomes into a tiny, non-developing cell called a polar body during anaphase I and disposal of half the remaining sister chromatids into a second polar body at anaphase II. This process is essential for generating a diploid zygote after fertilization in most animals. In *C. elegans*, spindle positioning occurs in three sequential steps. First, the nucleus of a maturing oocyte migrates toward the cortex at the junction with the younger oocyte (McCarter et al., 1999). Following nuclear envelope breakdown (NEBD) and the start of ovulation, the spindle translocates the remaining distance to the cortex (Yang et al., 2003). Spindle translocation is kinesin-1 dependent and APC (anaphase promoting complex)-independent (Yang et al., 2005). The metaphase spindle remains at the cortex in a parallel orientation, with each spindle pole equidistant from the cortex, until the initiation of APC-

2Corresponding author: Francis J. McNally, Department of Molecular and Cellular Biology, 149 Briggs Hall, University of California, Davis, Davis, CA 95616, phone: (530)754-8018, FAX: (530)752-3085, fjmcnally@ucdavis.edu.
[3]These authors contributed equally to this work.

dependent and dynein-dependent spindle rotation (Ellefson and McNally, 2009; van der Voet et al., 2009). During rotation, one spindle pole moves on a linear track toward the cortex, such that half of the chromosomes can be deposited in a polar body at anaphase.

The requirement for kinesin-1, a plus-end directed microtubule motor protein, and cytoplasmic dynein, a minus-end directed microtubule motor protein, is not due to interdependence of kinesin-1 and cytoplasmic dynein like that observed for peroxisome movements in *Drosophila* S2 cells (Kural et al., 2005). Kinesin-1 drives early spindle translocation in the absence of cytoplasmic dynein and cytoplasmic dynein drives late spindle translocation in the absence of kinesin-1. In addition, the localization of dynein on the spindle is unaffected by kinesin-1 inhibition (Yang et al., 2005; Ellefson and McNally, 2009). Thus the requirement for motors with opposite polarity to move the spindle in the same direction toward the cortex would be a paradox if both motors were directly bound to the spindle and moving on cytoplasmic microtubules. Cytoplasmic dynein accumulates on meiotic spindle poles at the same time as initiation of dynein-dependent movement of one spindle pole toward the cortex. In addition, dynein accumulation at spindle poles and dynein-dependent spindle movements both require the anaphase promoting complex (Ellefson and McNally, 2009). These results strongly indicate that cytoplasmic dynein plays a direct role in moving one spindle pole toward the cortex and leave unanswered the question of how a motor with opposite polarity can move the spindle in the same direction during early translocation.

To elucidate the mechanism of early spindle translocation, we first examined the localization of the kinesin-1 heavy chain, UNC-116, the kinesin-1 light chain, KLC-1, and KCA-1, in *C. elegans* meiotic embryos. KCA-1 is a *Caenorhabditis*-specific protein that binds to kinesin-1 and has an overlapping mutant phenotype with kinesin-1, indicating that it is required for kinesin-1's *in vivo* activity (Yang et al., 2005). Our results suggest that kinesin-1 directly transports yolk granules on cytoplasmic microtubules oriented toward the embryo interior and that the failure of spindle translocation in kinesin mutants is caused by a previously unrecognized failure in nuclear migration in maturing oocytes.

MATERIALS AND METHODS

C. elegans strains

In this study, wild type indicates either N2 or one of several integrated transgenic strains. The integrated GFP:YP170 (vitellogenin) strain DH1033 (*sqt-1(sc103) II; bIs1[vit-2::GFP + rol-6 (su1006)] X*) (Grant and Hirsh, 1999) was used for studies shown in Figures 3, 4, 5, 8 and 10. The integrated GFP::tubulin strain AZ244 (*unc-119(ed3) III; ruIs57[unc-119(+) pie-1::GFP::tubulin]*)(Praitis et al., 2001) was used for the studies shown in Figure 7. Strain FM78 was used as a negative control for anti-UNC-116 immunofluorescence. FM78 is *unc-116 (f122) dpy-17(e164) III; duIs1[unc-116:GFP + rol-6(su1006)]*. The *f122* allele of *unc-116* is a deletion that removes the coding sequences for the C-terminal 275 aa of UNC-116. In FM78, the lethal *f122* allele is complemented by an X-ray integrated multicopy array of *unc-116::GFP, rol-6*. No GFP fluorescence is discernable in the gonad or 1-celled embryos of FM78, most likely due to germline silencing of the multicopy insertion. In addition, the anti-UNC-116 antibody (Yang et al., 2005) recognizes only the C-terminal domain of UNC-116 and therefore should not recognize a truncated *f122* protein (Fig. S1). The *unc-116* mutant used for studies of cytoplasmic microtubule organization was HR399 *unc-36(e251) unc-116(f130) III*. The *f130* allele of *unc-116* is temperature-sensitive maternal effect lethal. Both *f122* and *f130* were isolated by Danielle Thierry-Mieg. FM10 was used in nuclear migration experiments. FM10 is *mei-1(ct46ct101) unc-13(e1091) daf-8(e1393)/hT2[bli-4(e937) let (h661) I; hT2/+ III*; ruIs57 [*unc-119*(+) *pie-1*::GFP:tubulin].

Immunofluorescence

Embryos were freeze-cracked and fixed with methanol/acetone as described (Miller and Shakes, 1995) except for embryos stained with anti-KLC-1 antibody which were fixed with methanol/formaldehyde as described (Basham and Rose, 2001). Antibodies specific for UNC-116 and KLC-2 were described previously (Yang et al., 2005). Rabbits were immunized with *E. coli*-expressed 6his-KLC-1 or MBP-KCA-1 and antibodies were blot affinity purified using the respective fusion proteins. Westerns with these antibodies are shown in Fig. S1. Imaging for most of Figures 1, 2 and 3 was carried out with an Olympus FV1000 confocal microscope with a PLAPON 60X 1.42 objective. Images in Fig. 2H and Fig. 6 were collected on an Applied Precision DeltaVision deconvolution microscope with an Olympus 60X 1.4 objective and a CoolSnapHQ CCD (Photometrics/Roper) with no binning. Images in Fig. 8 were obtained with an Olympus DSU spinning disk confocal using a 60X Plan Apo 1.42 objective and a Hamamatsu Orca R2 CCD.

In utero filming of meiotic embryos

Adult hermaphrodites were anesthetized with Tricaine/tetramisole as described (McCarter et al., 1999; Kirby et al., 1990) and gently mounted between a coverslip and a thin agarose pad on a slide. Mineral oil or petroleum jelly was used to reduce evaporation at the edge of the coverslip. Images for Figures 4, 5, 7 and 10 were acquired with a Perkin-Elmer UltraView spinning disk confocal microscope equipped with an Olympus 100X Plan Apo 1.35 objective, Hamamatsu Orca ER CCD and Slidebook acquisition software. 2×2 binning was used for all live imaging. All quantitative analysis was carried out with Ivision software (Biovision) or Image J.

Single particle tracking

The Manual Tracking plugin for Image J was used for single particle tracking. Maximum intensity projections were used to display particle tracks occurring at different times in a single image (Fig. 5). The beginning of a “paused state” was defined as an instantaneous velocity of 0 in 3 consecutive frames. The end of a paused state was defined as a positive instantaneous velocity value for 2 consecutive frames.

RNA interference

All RNA interference was by feeding (Timmons et al., 2001). KCA-1 was depleted with clone I-2I09, RAB-7 with clone II-8G13 and FZY-1 with clone II-4O16 (MRC Gene Services, Kamath et al., 2003). UNC-116 was depleted with pFM1040 consisting of a 1.5 kb BamHI-SalI fragment of an UNC-116 cDNA inserted into L4440 (Timmons et al., 2001). Profilin was depleted with pFM748 consisting of a full-length PFN-1 cDNA inserted as a BamHI-NotI fragment into L4440. CLS-2 was depleted with clone pFM529 (Yang et al., 2003). Feeding was carried out for 24–36 hrs at 25°C.

Imaging of GFP:KCA-1, mCherry:KCA-1 and mCherry:KLC-1

The *kca-1* gene was PCR amplified from genomic DNA introducing a 5′ NheI site and a 3′ SpeI site. This product was cloned into the SpeI site of the pie-1/GFP vector pIC26 (Cheeseman and Desai, 2005) to produce pFM1092 and the pie-1/mCherry vector pAA64 to produce pFM1093. The same strategy was used to clone the *klc-1* gene into pAA64 producing pFM1128. Transgenic worm lines were generated by micro-particle bombardment of *unc-119* mutant worms (Praitis et al., 2001). Transgenic lines were imaged immediately after they were isolated and carefully compared with N2 to control for autofluorescence, which was particularly noticeable in GFP wavelengths in the distal gonad. Expression of the transgenes was completely silenced within 2 weeks. *mut-16(RNAi)*, which has been reported to de-silence germline transgenes (Kim et al., 2005) and co-suppressed transgenes (Robert et al., 2005), was

then used to de-silence transgene expression. Data shown includes images captured before transgene silencing and after de-silencing. Localization patterns were identical before silencing and after de-silencing.

Filming of nuclear migration

Diakinesis oocytes are extremely prone to arrest when worms are anesthetized and mounted for time-lapse imaging. Therefore, only time-lapse sequences in which germinal vesicle breakdown and ovulation occurred were used for the analysis shown in Fig. 9 and shuttered brightfield imaging with minimal illumination intensity was used. The velocity of wild-type nuclear migration was determined from 7 time-lapse sequences of N2 worms and 6 from FM10 worms. No difference in migration velocity was observed between these strains but the FM10 worms ovulated under our imaging conditions with much higher frequency than N2.

RESULTS

Kinesin-1 heavy chain, KLC-1 and KCA-1 are concentrated in the middle of meiotic embryos and reduced in concentration at the cortex and meiotic spindle

To test whether the kinesin-1 heavy chain, UNC-116, co-localizes with meiotic spindles, meiotic embryos were fixed and stained with a previously described anti-UNC-116 antibody (Yang et al., 2005 and Fig. S1). In 23/23 meiotic embryos, anti-UNC-116 staining was diffuse, suggesting cytoplasmic localization, but the UNC-116 was concentrated in the middle of the embryo and reduced in concentration in a region close to the cortex (Fig. 1A, B). In 17/17 meiotic embryos that were double labeled with anti-UNC-116 antibody and anti-α tubulin antibody, anti-UNC-116 staining was reduced or absent from the meiotic spindle (Fig. 1B). Several lines of evidence indicate that this is the true localization of kinesin-1 in living meiotic embryos. First, anti-UNC-116 staining of meiotic embryos from an *unc-116* mutant with reduced levels of UNC-116 protein (FM78, see Materials and Methods and Fig. S1) was 3.5 fold dimmer than staining of wild-type meiotic embryos and was uniform across the embryo (n=4 mutant, 10 wt, Fig. 1C). Second, anti-UNC-116 staining was inverted, with brighter staining at the cortex, or uniform throughout the cytoplasm in 15/15 meiotic embryos that were depleted of the kinesin-1 regulator, KCA-1 (Fig. 1D). Third, the concentration of UNC-116 in the middle of the embryo was specific for meiotic embryos; UNC-116 staining extended uniformly to the cortex in mitotic embryos (Fig. 1E). Fourth, the specific concentration in the middle of meiotic embryos was also observed with antibody staining and fluorescent protein fusions to KLC-1 and KCA-1, proteins that form a complex with UNC-116 *in vitro* and which have overlapping mutant phenotypes with UNC-116 (Yang et al., 2005).

To determine the subcellular localization of the kinesin-1 light chain, KLC-1, we constructed a transgenic worm strain that expresses mCherry:KLC-1 from the *pie-1* promoter by micro-particle bombardment (Praitis et al., 2001). Living meiotic embryos were identified *in utero* in anesthetized worms by brightfield microscopy, then imaged by spinning disk confocal microscopy. In 12/12 meiotic embryos, mCherry:KLC-1 was diffuse but 2.0 +/− 0.3 fold more concentrated in the middle of the embryo than near the cortex (Fig. 2A). mCherry:KLC-1 was uniformly distributed in 12/12 mitotic embryos (1.1 +/− 0.1 fold brighter in the middle relative to the cortex; Fig. 2A). The cytoplasmic fraction of an mCherry:histone H2B fusion protein was uniformly distributed in 12/12 meiotic embryos (1.0 +/− .05 brighter in the middle relative to the cortex; Fig. 2B), indicating that the apparent concentration in the central cytoplasm is not an optical artifact nor is it a property of mCherry itself. To confirm that endogenous KLC-1 was localized the same as the mCherry:KLC-1 fusion protein, fixed embryos were labeled with a KLC-1-specific antibody (Fig. S1). 5/9 wild-type meiotic embryos exhibited brighter staining in the middle of the embryo (Fig. 2C, avg. 1.4 fold brighter in the middle than the cortex) while the remaining embryos exhibited uniform cytoplasmic staining. 4/5 *unc-116* mutant (FM78)

meiotic embryos exhibited uniform or inverted KLC-1 staining (Fig. 2D, 1.3 fold brighter at the cortex than in the middle of the embryo).

To determine the subcellular localization of the kinesin-1 regulator, KCA-1, we constructed a transgenic worm strain that expresses GFP:KCA-1 from the *pie-1* promoter by micro-particle bombardment (Praitis et al., 2001). In 13/13 living meiotic embryos, GFP:KCA-1, like mCherry:KLC-1 and UNC-116, was diffuse but concentrated in the middle of the embryo and reduced in concentration in a region near the cortex (1.6 +/− .2 fold brighter in the middle of the embryo relative to the cortex; Fig. 2E). GFP:KCA-1 was uniformly distributed in 12/12 mitotic embryos (1.0 +/− .07 fold brighter in the middle of the embryo relative to the cortex; Fig. 2F) and the cytoplasmic pool of a GFP:histone H2B fusion protein was uniformly distributed in 12/12 meiotic embryos (1.05 +/− .05 fold brighter in the middle of the embryo relative to the cortex, Fig. 2G), indicating that the apparent concentration in the central cytoplasm is not an optical artifact nor is it a property of GFP itself. To further test whether endogenous KCA-1 localizes in the middle of the embryo, meiotic embryos were fixed and stained with an anti-KCA-1 antibody (Fig. S1). Anti-KCA-1 immunofluorescence showed bright cytoplasmic staining in the middle of 27/29 meiotic embryos (Fig. 2H). Anti-KCA-1 staining was 2 fold dimmer and uniform in 7/7 *kca-1(RNAi)* embryos (Fig. S2). Taken together, these results indicate that UNC-116, KLC-1 and KCA-1 are all concentrated in the cytoplasm in the middle of meiotic embryos and reduced or absent from the cytoplasm near the cortex and the meiotic spindle. Quantitatively, the relative enrichment in the middle of meiotic embryos varied from extreme cases (4.8 fold enrichment of UNC-116 in Fig. 1A, 3.5 fold enrichment of KLC-1 and KCA-1 in Fig. 2I and 2J) to much shallower gradients (1.35 fold enrichment of KLC-1 in Fig. 2C). However, this concentration of kinesin-1 subunits in the middle of meiotic embryos was always dependent on UNC-116 and KCA-1 and was never observed in mitotic embryos.

Yolk granules are packed into the middle of meiotic embryos where UNC-116 is concentrated

The concentration of kinesin-1 subunits in a diffuse central mass within meiotic embryos was unexpected and suggested that kinesin-1 might transport cargoes other than the spindle. We previously found that membranous organelles within meiotic embryos move in a circular pattern in a microtubule-dependent manner (Yang et al., 2003). To test whether kinesin's concentration in the center of meiotic embryos might be related to movements of membranous organelles, we first analyzed the position of yolk granules labeled with GFP:vitellogenin, a protein that is endocytosed by maturing oocytes (Grant and Hirsh, 1999). *C. elegans* yolk granules can be described as modified lysosomes because they depend on the same sorting machinery as lysosomes in other species (Grant and Hirsh, 1999; Poteryaev et al., 2007) and because they contain the acid protease cathepsin L (Britton and Murray, 2004), but like yolk granules in other species, they do not proteolyze vitellogenin until later in development (Fagotto et al., 1995). Like UNC-116, yolk granules were concentrated in the middle of meiotic embryos and excluded from a region near the cortex including the spindle (Fig. 3A and B). In 10/10 wild-type meiotic embryos, yolk granules were concentrated in the same region of the embryo as UNC-116 (Fig. 3A). Like UNC-116, yolk granules were excluded from the spindle in 24/24 wild-type meiotic embryos (Fig. 3B). In 26/26 *kca-1(RNAi)* meiotic embryos, yolk granules were no longer packed toward the center and in most cases exhibited an inverse pattern of yolk granules concentrated at the periphery of the embryo (Fig. 3C). KCA-1-dependent and UNC-116-dependent central concentration of yolk granules was also observed in living meiotic embryos (Figure S3), therefore this pattern is not an artifact caused by contraction and swelling during methanol fixation and rehydration. Like kinesin-1, yolk granules were evenly distributed in wild-type mitotic embryos (Fig. 3D). Thus kinesin-1 and yolk granules are both concentrated in the middle of meiotic embryos in a kinesin-1 and KCA-1-dependent manner, but the kinesin-1 heavy chain, UNC-116, is not restricted to the surface of the yolk granules

(Fig. 3A). To eliminate the possibility that surface concentration was not observed because the yolk granules are small relative to the thickness of a confocal optical section, we used *rab-7 (RNAi)* to trap vitellogenin-containing vesicles as endosomal intermediates (Poteryaev et al., 2007), which are much larger than mature yolk granules. The surface of these large vesicles, which are also concentrated in the middle of meiotic embryos (Fig. S4), could be resolved clearly. UNC-116 still did not appear concentrated on these membrane surfaces (Fig. 3E). Failure of endogenous kinesin-1 to appear concentrated on the surface of cargo is extremely common. For example, endogenous kinesin-1 does not appear to concentrate on the surface of mitochondria in the majority of mammalian cultured cells (Glater et al., 2006) but endogenous kinesin-1 is efficiently recruited to mitochondria when its cargo adaptors miro and Milton are over-expressed (Glater et al., 2006; Wang and Schwarz, 2009), even though an endogenous kinesin-1, miro, Milton complex is present in these cells (Wang and Schwarz, 2009). Mitochondrial movements, however, are completely dependent on kinesin-1, miro and Milton (Glater et al., 2006). A common explanation for this is that a small number of kinesin-1 molecules transiently associate with microtubules and cargo while the majority of kinesin-1 molecules are in a cytoplasmic, auto-inhibited state (Hackney and Stock, 2000).

Yolk granules move in a kinesin and KCA-1 dependent manner

To test whether yolk granule movements are dependent on kinesin-1 and KCA-1, time-lapse spinning disk confocal microscopy was conducted on meiotic embryos containing GFP:vitellogenin-labeled yolk granules. Embryos were filmed for an average of 14 min beginning immediately after spermatheca exit. In 7/7 wild-type embryos, yolk granules moved in an apparently circular pattern around the embryo (Video 1 and 2). Maximum intensity projections of time-lapse images collected at 4 sec intervals over 67 sec revealed long arcs suggesting circular movement (Fig. 4A). Projections from mitotic embryos, diakinesis oocytes, *unc-116 (RNAi)* or *kca-1(RNAi)* meiotic embryos (Fig. 4B, C, D, E) revealed no arcs, suggesting a lack of long range movement. Instead, yolk granules had an increased apparent diameter in a time series projection relative to a single time point. To help interpret these projections, we followed 25 randomly chosen yolk granules and found that in wild-type meiotic embryos, 52% of yolk granules were present in only a single frame, indicating that they remained in the same focal plane for less than the 4 sec interval between images. The remaining 48% of yolk granules remained in focus for an average of 15 sec. In contrast, all of the yolk granules in an adjacent mitotic embryo or in a *kca-1(RNAi)* meiotic embryo remained in focus for multiple frames (avg 46 sec and 32 sec respectively). These results suggest that the majority of yolk granules in mitotic embryos or *kca-1(RNAi)* meiotic embryos are undergoing Brownian motion in a limited volume that is described by the increased diameter in a projection of a time series (Fig. 4). In contrast, the majority of yolk granules in a wild-type meiotic embryo are undergoing rapid movements that remove them from the focal plane so that they are represented by a small spot in a projection of a time series. The arcs generated in a time series projection of a wild-type meiotic embryo thus indicate rapid movements of a subset of yolk granules in a circular pattern. This movement occurs in meiotic but not mitotic embryos, is dependent on UNC-116 and KCA-1, but does not require a profilin-dependent actin cytoskeleton (Fig. 4F). Consistent with the idea that this movement is generated by kinesin-mediated transport on microtubules, this movement was blocked by tubulin (RNAi) (Yang et al., 2003).

To measure the velocity of the subset of yolk granules that remained in focus for multiple frames in wild-type meiotic embryos, we first used kymograph analysis along a manually selected line in the direction of apparent movement (Fig. S5). In the example shown, multiple diagonal lines indicate multiple different yolk granules moving along the same line at different times, each at a velocity of 0.26 +/− .04 μm/sec (n=6 embryos, 8 kymographs). Kymographs of 6/6 *kca-1(RNAi)* or 6/6 *unc-116(RNAi)* meiotic embryos revealed oscillating vertical lines, consistent with Brownian motion within a limited volume (Fig. S5). Because these movements

were observed in meiotic embryos but not in mitotic embryos and because these movements depended on KCA-1 and UNC-116, just like the central cytoplasmic concentration of UNC-116 and yolk granules, we suggest that the observed movements of yolk granules may cause the concentration of kinesin-1 and yolk granules in the middle of meiotic embryos. This implies that net, plus-end directed microtubule-based transport is directed away from the cortex.

To directly test for kinesin-dependent transport of yolk granules away from the cortex, we analyzed a time series of GFP:vitellogenin images of a meiotic embryo collected at 300 ms intervals. A total of 41 yolk granules were tracked moving with an average instantaneous velocity of 0.54 μm/sec (range 0.21–0.98 μm/sec). 18 yolk granules were tracked moving on inward trajectories from near the cortex (Fig. 5B). Most of these tracks followed arcs parallel to the cortex (Fig. 5B and C). Very few tracks were oriented directly toward the cortex (white and pink tracks at top of Fig. 5C). If particle tracks correspond to direct transport of yolk granules on microtubules, then these tracks demonstrate the existence of microtubules near the cortex extending diagonally inward. Several observations support the hypothesis that these movements represent direct transport of yolk granules on microtubules rather than passive movements with flowing cytoplasm.

Yolk granule movements are consistent with direct transport on microtubules and not with passive flow

If the long curved arcs in time-series projections were caused by passive movement with cytoplasmic flow, then the velocity of particles in the middle of the embryo would be slower than the velocity of particles on the longer arcs at the edge of the embryo. To test this, we tracked 4 adjacent yolk granules in the middle of the embryo and 5 adjacent particles on the edge of the same embryo. Each group of yolk granules appeared to be moving along the projection arcs. If velocity was measured as the net displacement in a straight line over the time interval that the yolk granule remained in focus, the yolk granules in the middle of the embryo moved at a velocity of 0.08 +/− .02 μm/sec while the yolk granules at the edge of the embryo moved at a velocity of 0.3 +/− .1 μm/sec. However, monitoring instantaneous velocities at 300 ms time resolution revealed that the “slow” yolk granules in the middle of the embryo alternated between a paused state and a moving state. Instantaneous velocity in the moving state was 0.4 +/− .07 μm/sec (n= 4 yolk granules, 14 moving episodes). Instantaneous velocity of yolk granules at the edge of the embryo was 0.5 +/− .08 μm/sec (n = 5 yolk granules). Thus yolk granules in the middle and at the edge of the embryo move with the same instantaneous velocity, consistent with direct transport on microtubules and inconsistent with cytoplasmic flow. The saltatory, starting and stopping, behavior of yolk granules in the middle of the embryo is also consistent with direct transport by kinesin and inconsistent with cytoplasmic flow.

Several other features consistent with direct transport on microtubules were revealed during single particle tracking at 300 ms time resolution. Some yolk granules moved on trajectories nearly perpendicular to the projection arcs (Fig. 5D). Figs. 5E–G show a yolk granule (shown in pink) undergoing Brownian motion while two adjacent yolk granules move on linear tracks. It would be impossible for two yolk granules to move with cytoplasmic flow while an adjacent yolk granule is exhibiting Brownian motion without net displacement. Fig. 5H shows a yolk granule making a 90° turn, an event consistent with a yolk granule switching from one microtubule to an intersecting microtubule, but not consistent with cytoplasmic flow. 5/19 yolk granules tracked through a high frame rate time-lapse sequence of a second wild-type embryo changed direction while adjacent yolk granules continued moving in their original direction. If yolk granules were moving passively with cytoplasmic flow, they should undergo Brownian motion as they flow. Instead, single particle tracks (Fig. 5) are narrow enough to be explained by lateral pivoting of a yolk granule as it moves along a microtubule. Brownian motion would result in wider lateral movements as in Fig. 5F. The individual behaviors of yolk granules are

thus consistent with kinesin-driven transport on microtubules rather than with kinesin-dependent cytoplasmic flow.

Parallel microtubules extend inward from the cortex

Direct transport of yolk granules on microtubules by kinesin-1 would require the presence of parallel microtubules extending diagonally inward from the cortex. Analysis of wild-type meiotic embryos by fixed anti-tubulin immunofluorescence and 3D deconvolution microscopy indeed revealed the presence of parallel cytoplasmic microtubules extending diagonally inward from the cortex (Fig. 6A and B) or parallel microtubules at the surface of the cortex (Fig. 6C) in 29/36 wild-type embryos. Analysis of the density of microtubules throughout the embryo revealed a higher density near the cortex and a lower density in the middle of the embryo in 25/34 wild-type meiotic embryos (Fig. 6E and G). Microtubules in 12/14 *kca-1(RNAi)* meiotic embryos appeared more randomly oriented (Fig. 6D and F) with no enrichment of microtubules at the cortex (Fig. 6H). Similar results were obtained in *unc-116(f130)* mutant embryos (not shown).

The arrangement of microtubules shown in Fig. 6 and the movement of yolk granules shown in Figure 4 and Video 1 and 2 are consistent with the model shown in Fig. 7A. Inward transport of yolk granules by kinesin-1 would concentrate yolk granules in the middle of the embryo. As the embryo becomes packed with yolk granules that increase in number due to endocytosis of vitellogenin, the microtubules with minus ends anchored at the cortex would be forced to pivot outward, causing the start of circular streaming and the concentration of microtubules at the cortex. When microtubule plus ends pivot along the long axis of the oval embryo (Fig. 7A upper right; Fig. 6A and B), circular streaming of yolk granules would occur in the long axis of the embryo (Video 1). When microtubules pivot along the short axis of the embryo (Fig. 7A lower right; Fig. 6C), circular streaming occurs in the short axis of the embryo (Video 2).

To further test this model, we conducted time-lapse imaging of GFP:tubulin-labeled cytoplasmic microtubules in living meiotic embryos. Parallel microtubules extending diagonally inward were visible in most time-lapse sequences (Fig. 7B) and appeared to be oriented in the direction of streaming. Accurate tracking of the movements of individual cytoplasmic microtubules was not possible but their movement can be documented indirectly. 1.5 second exposures were required to image these microtubules and very few microtubules were observed in living meiotic embryos compared with adjacent oocytes (Fig. 7C) or fixed meiotic embryos (Fig. 6). When 34 individual microtubules in a meiotic embryo were tracked, 74% could only be identified in a single frame. The remaining 26% could be tracked for an average of 5 +/− 2 sec. In striking contrast, 100% of the microtubules in an adjacent diakinesis oocyte could be tracked through multiple frames (avg. 9 +/− 5 sec, n= 28). These observations indicate that the majority of cytoplasmic microtubules in meiotic embryos are moving significant distances during the 1.5 sec exposures required to observe them. These observations are consistent with microtubules that constantly pivot in 3 dimensions about their minus end anchorage point at the cortex.

Central packing of yolk granules is uncoupled from spindle translocation by *cls-2(RNAi)*

Cytoplasmic microtubules with minus ends anchored at the cortex (Fig. 7A) could explain the concentration of yolk granules and kinesin-1 subunits in the central cytoplasm but do not explain why outward translocation of the meiotic spindle to the cortex is dependent on kinesin-1 (Yang et al., 2005). One possibility is that tight packing of yolk granules in the middle of the embryo passively forces the meiotic spindle outward. If this model were correct, early translocation of the spindle to the cortex should only be observed in embryos with centrally packed yolk granules. In an earlier study (Yang et al., 2003), we reported that spindle translocation was normal but circular streaming of membranes (observed by DIC microscopy)

was defective in *fzy-1(RNAi)* and in *cls-2(RNAi)* embryos. To specifically assay for central packing of yolk granules, the APC subunit, FZY-1, and the microtubule-binding protein, CLS-2, were depleted from worms expressing GFP:vitellogenin. In 12/14 *fzy-1(RNAi)* metaphase I meiotic embryos, spindles were at the cortex and yolk granules were packed in the middle of the embryo as in wild type (Fig. 8A). In contrast, 22/24 *cls-2(RNAi)* metaphase I meiotic embryos had yolk granules that were dispersed to the cortex and the spindles were at the cortex (Fig. 8B). The *cls-2(RNAi)* embryos demonstrate that spindle translocation cannot be caused by the central packing of yolk granules.

Kinesin-1 is required for nuclear migration in maturing oocytes

The nucleus of a maturing oocyte migrates toward the cortex at the junction with the younger oocyte (the future anterior pole of the embryo) before nuclear envelope breakdown, spindle assembly and ovulation (McCarter et al., 1999). If *unc-116(RNAi)* oocytes were defective in this process, then spindles might assemble further from the cortex than in wild type and the observed spindle translocation effects might be caused by this increased distance from the cortex. By time-lapse, bright-field imaging of anesthetized worms (see Materials and Methods), we found that in 13/13 wild-type worms, the nucleus of the -1 oocyte migrated to the junction with the -2 oocyte at a velocity of .006 +/− .001 μm/sec (Fig. 9A). In worms depleted of kinesin-1 subunits, the nucleus of the -1 oocyte did not move toward the membrane junction with -2 oocyte (Figure 9B and C). The failure in nuclear migration observed by time-lapse imaging was confirmed by measurements of the distance of the nucleus from the cortex at the time of nuclear envelope breakdown (Table 1). The nucleus still became asymmetrically positioned within the -1 oocyte without any nuclear migration, apparently due to asymmetric growth of the oocyte (Fig. 9B and C). The idea that failed nuclear migration might lead to spindle assembly further from the cortex is supported by our previous measurements of the distance between the spindle and cortex at the time that the zygote exits the spermatheca into the uterus (Yang et al., 2005). In those measurements, spindles were twice as far from the cortex in *unc-116(RNAi), klc-1; klc-2(double RNAi)* or *kca-1(RNAi)* worms than in wild-type worms.

Kinesin-1 localization and yolk granule movements change dramatically during ovulation

Inward movement of yolk granules and outward movement of the spindle by the same microtubule motor would only be a paradox if these movements occurred simultaneously. Because kinesin-1 appears to move the nucleus toward one cortex in diakinesis oocytes, we analyzed time-lapse images of yolk granules captured at 300 ms time intervals in diakinesis oocytes of wild-type worms to see how their movements differed from meiotic embryos. 98% of yolk granules could be tracked through multiple frames and 83% (n=40) were stationary over a 15 sec time interval (Fig. 10A and B) in contrast to the rapidly moving yolk granules in meiotic embryos (Figs 4 and 5). Only 17% of yolk granules exhibited intermittent, fast linear movements (Fig. 10C) and the movements occurred in multiple directions. To address why kinesin-dependent transport of yolk granules is suppressed in diakinesis oocytes, we examined the localization of kinesin-1 subunits in the most mature diakinesis oocyte. In living worms, mCherry:KCA-1, GFP:KCA-1 and mCherry:KLC-1 were concentrated in discrete but unidentified structures (Fig. 10D). These structures were not concentrated in the middle of the oocyte nor excluded from the cytoplasm near the cortex as was the diffuse, cytoplasmic pool of these proteins in meiotic embryos. The punctate localization of kinesin subunits in the -1 oocyte thus corresponds with inactive yolk granule transport and active nuclear migration while the cytoplasmic localization in meiotic embryos corresponds to active yolk granule transport. These observations indicate a major change in kinesin's activity during maturation and ovulation. These observations also suggest a solution to the apparent microtubule polarity paradox. If the organization of cytoplasmic microtubules changes between a diakinesis oocyte

and a meiotic embryo, then kinesin-1 could directly drive nuclear migration to the anterior cortex in oocytes and inward movement of yolk granules in meiotic embryos.

DISCUSSION

Our results indicate that kinesin-dependent inward transport of yolk granules increases at ovulation, possibly due to activation of kinesin-1. Because yolk granules move away from the cortex on linear tracks, without Brownian motion, at velocities similar to those of kinesin-driven vesicle movements in neurons (Vale et al., 1995; Pilling et al., 2006), and because kinesin subunits concentrate in the middle of the embryo with the yolk granules, we propose that yolk granules are direct cargos of kinesin-1. Kinesin-1 subunits did not appear concentrated at the surface of the yolk granules, just as they did not appear concentrated at the surface of mitochondria that they clearly transport (Glater et al., 2006). The longest inward movements of yolk granules that we observed in our high-speed imaging (Fig. 5) lasted approximately 15 sec. If each kinesin-1 molecule dissociated from the yolk granule as it ran off the end of a cytoplasmic microtubule, it would be expected to return to a cytoplasmic, auto-inhibited state (Hackney and Stock, 2000) and diffuse freely before engaging a new yolk granule and a new microtubule for another 15 sec run. If each kinesin-1 molecule spends more time in the cytoplasmic state than in the transport state, but the net transport rate exceeds the backward diffusion rate, this would explain the observed concentration of kinesin-1 subunits in the cytoplasm in the middle of the embryo. If inward movement of yolk granules is indeed due to direct kinesin-driven transport on cytoplasmic microtubules, this implies that *C. elegans* meiotic embryos have microtubules with minus ends anchored at the cortex and plus ends oriented toward the interior. This microtubule arrangement has been directly demonstrated by hook decoration in *Xenopus* oocytes (Pfeiffer and Gard, 1999) and has been proposed in *Drosophila* oocytes (Cha et al., 2002).

We speculate that inward transport collapses into apparent circular streaming when membrane vesicles become so packed in the middle of the embryo that they force outward pivoting of cytoplasmic microtubules that have minus ends anchored at the cortex. Outward pivoting of cortical microtubules would explain the kinesin-dependent concentration of cytoplasmic microtubules at the cortex and the conversion of inward movement to circular movement.

The action of kinesin-1 also results in the movement of the meiotic spindle (Yang et al., 2005) in the opposite direction, outward toward the cortex. Because the spindle moves in the opposite direction, at a velocity 100X slower than purified kinesin-1, and because kinesin-1 subunits are present at reduced concentrations near the meiotic spindle and cortex, we suggest that the outward movement of the spindle may be indirectly caused by kinesin-1. One possible indirect mechanism is that kinesin-1 never exerts force on the spindle, but instead moves the nucleus to the cortex before spindle assembly. Our data indicate that in the absence of kinesin-1, the nucleus indeed does not migrate to the cortex and as a result, the spindle assembles at a greater distance from the cortex. This increased distance might be too far for a kinesin-independent spindle translocation mechanism to function. A second function of kinesin-1 is suggested by the observation that, in kinesin-depleted embryos, the metaphase II spindle sometimes drifts several microns from the cortex after dynein-mediated late translocation of the anaphase I spindle to the cortex (Yang et al., 2005). This result suggests that kinesin-1 is anchoring the meiosis II spindle at the cortex long after nuclear envelope breakdown. We propose that after kinesin-1 drives nuclear migration in the most mature diakinesis oocyte, it continues to anchor the nucleus and later the spindle to the cortex throughout meiosis I and II. Anchoring, but not migration, of the nucleus to the oocyte cortex by kinesin-1 occurs in *Drosophila* oocytes (Januschke et al., 2002) and cortical anchoring of the spindle by kinesin-1 in *C. elegans* is not inconsistent with simultaneous inward transport of yolk granules by kinesin-1.

Centripetal packing of yolk granules has been observed in the eggs of many phyla and may be important for clearing a region below the cortex to allow important subcortical events like cortical granule exocytosis. In zebrafish zygotes, yolk granules that were initially spherical and evenly distributed throughout the unfertilized oocyte become packed so tightly together that they have flattened interfaces (Beams et al., 1985; Fernandez et al., 2006). During this packing, a yolk-free layer forms just below the cortex, all around the zygote (Roosen-Runge, 1938; Leung et al., 2000) and cortical granules concentrate in this zone (Mei et al., 2009). In annelid eggs, yolk granules are transported away from the cortex as mitochondria (Fernandez at al., 1998) and mRNAs (Jeffery and Wilson, 1983) are concentrated in the resulting yolk-free cytoplasm under the cortex. In *C. elegans* meiotic embryos, cortical granules that contain caveolin-1 (CAV-1) and chondroitin proteoglycans (Sato et al., 2008) are translocated to the subcortical, yolk-free zone during ovulation (Sato et al., 2006). These vesicles fuse with the plasma membrane at the metaphase I-anaphase I transition (Sato et al., 2008), releasing the proteoglycans into the eggshell. CAV-1 is then re-internalized by endocytosis and the resulting endosomes remain in the cortical yolk-free zone during meiosis II (Sato et al., 2006). A different class of endosomes containing MBK-2, EGG-3 and chitin synthase (Maruyama et al., 2007) are formed 4 min after initiation of anaphase I chromosome segregation (McNally and McNally, 2005) and these vesicles are also concentrated in the yolk-free cortical zone during meiosis. We speculate that clearing yolk granules from the egg cortex may be important for allowing regulated waves of secretion and endocytosis in many species.

Results in *Drosophila* oocytes indicate that fast circular streaming of yolk granules requires fast kinesin-dependent transport but that fast circular streaming is not an essential process. Just as in *C. elegans* meiotic embryos, fast circular streaming in stage 10 *Drosophila* oocytes is kinesin-1-dependent and actin-independent. A kinesin-1 point mutation that results in slow motility in vitro and blocks fast circular streaming in vivo, however, allows normal localization of oskar RNA and embryonic viability (Serbus et al., 2005). We propose that fast circular streaming is an indirect consequence of fast, unidirectional, inward transport of organelles by kinesin-1. Mutations that slow the motor's velocity allow transport of essential cargo but not the phenomenon of circular streaming. This might explain why *fzy-1(RNAi)* causes partial inhibition of fast circular streaming (Yang et al., 2003) but does not prevent inward packing (Fig. 8). In this model, we would expect yolk granules to be packed into the middle of stage 10 *Drosophila* oocytes and expect to see a discrete subcortical layer free of yolk granules. A discrete subcortical layer of stationary cytoplasm has in fact been reported in stage 10 *Drosophila* oocytes (Gutzeit and Koppa, 1982) and this layer may be analogous to the subcortical region of a *C. elegans* meiotic embryo where stationary cortical granules and stationary, CAV-1-labeled endosomes are concentrated (Sato et al., 2006). An unidentified class of membrane vesicles is packed into the middle of the *Drosophila* oocyte. The central packing of these vesicles was proposed to be due to centripetal microtubule-dependent transport because direct contact between these vesicles and microtubules was observed in electron micrographs (Theurkauf et al., 1992). It is possible that a yolk-free subcortical zone has not been reported in stage 10 *Drosophila* oocytes because of the methods used to image yolk granules. For example, endocytosis of Trypan blue (Serbus et al., 2005) may label multiple classes of endosomes, including both stationary subcortical endosomes and inwardly transported yolk granules.

If the cytoplasmic microtubules in *C. elegans* meiotic embryos indeed have minus ends anchored at the cortex like those demonstrated in *Xenopus* oocytes (Pfeiffer and Gard, 1999), this organization would provide tracks for dynein-mediated rotation of anastral meiotic spindles (Ellefson and McNally, 2009). This might be essential for meiotic spindles that do not have the centrosome-based astral microtubule arrays thought to drive dynein-dependent cortical pulling in other cell types (Sheeman et al., 2003).

A role for kinesin-1 in nuclear migration is not unexpected since it is required for nuclear migration in *C. elegans* hyp7 cells where it binds directly to the outer nuclear envelope KASH protein UNC-83 (Meyerzon et al., 2009). UNC-83 is not expressed in the germline where the KASH proteins ZYG-12 (Malone et al., 2003) or KDP-1 (McGee et al., 2009) might mediate kinesin-1 interaction with the nuclear envelope. ZYG-12 targets cytoplasmic dynein to the nuclear envelope in oocytes and dynein/ZYG-12 is required for the organization of membranes and gross nuclear positioning in oocytes (Zhou et al., 2009). In contrast, kinesin-1/KCA-1 is not required for oocyte membrane organization or centering diakinesis nuclei (Fig. 9 and Yang et al., 2005) but is specifically required for migration of the nucleus to the anterior cortex of the most mature oocyte. Even in the complete absence of nuclear migration toward the cortex, nuclei become asymmetrically positioned in the -1 oocyte, possibly because the -1 oocyte grows asymmetrically toward the spermatheca (Fig. 9B and C). To determine the molecular mechanism of kinesin-dependent nuclear migration in the oocyte, it will be important to determine the polarity of microtubules during migration. The arrangement and dynamics of oocyte microtubules has been shown to change during maturation in response to MSP signaling from sperm in the spermatheca (Harris et al., 2006). The microtubule minus end marker, ϒ-tubulin, is found at the cortex and nuclear envelope of diakinesis oocytes (Zhu et al., 2009) and the amount of ϒ-tubulin on the nuclear envelope increases dramatically just before nuclear envelope breakdown (McNally et al., 2006). Establishing when these changes occur relative to nuclear migration may illuminate kinesin-1's role in migration.

Supplementary Material

Refer to Web version on PubMed Central for supplementary material.

Acknowledgments

We thank Danielle Thierry-Mieg and Paul Mains for *unc-116(f122)* and *unc-116(f130)*. We thank Heather Brown and Yishi Jin for the *unc-116*::GFP extrachromosomal array, Yuji Kohara for cDNA clones, Barth Grant for GFP:YP170 strains, Anjon Audhya for pAA64, Ian Cheeseman for pIC26, Lesilee Rose, Ingrid Brust-Mascher and Jon Scholey for use of facilities. We thank Dmitrey Kolesnikov and Jennifer Milan for technical assistance.

This work was supported by grant R01GM079421 from the National Institute of General Medical Sciences.

References

Basham SE, Rose LS. The *Caenorhabditis elegans* polarity gene ooc-5 encodes a Torsin-related protein of the AAA ATPase superfamily. Development 2001;128:4645–4656. [PubMed: 11714689]

Beams HW, Kessel RG, Shih CY, Tung HN. Scanning electron microscopy studies on blastodisc formation in the zebrafish, Brachydanio rerio. J Morphol 1985;184:41–49.

Britton C, Murray L. Cathepsin L protease (CPL-1) is essential for yolk processing during embryogenesis in *Caenorhabditis elegans*. J Cell Sci 2004;117:5133–5143. [PubMed: 15456850]

Cha BJ, Serbus LR, Koppetsch BS, Theurkauf WE. Kinesin I-dependent cortical exclusion restricts pole plasm to the oocyte posterior. Nat Cell Biol 2002;4:592–8. [PubMed: 12134163]

Cheeseman I, Desai A. A combined approach for the localization and tandem affinity purification of protein complexes from metazoans. Sci STK 2005 January 11;:pl1.

Ellefson ML, McNally FJ. Kinesin-1 and Cytoplasmic Dynein Act Sequentially to Move the Meiotic Spindle to the Oocyte Cortex in *C. elegans*. Mol Biol Cell 2009;20:2722–2730. [PubMed: 19357192]

Fagotto F. Regulation of yolk degradation, or how to make lysosomes sleepy. J Cell Sci 1995;108:3645–3647. [PubMed: 8719870]

Fernandez J, Olea N, Ubilla A, Cantillana V. Formation of polar cytoplasmic domains (teloplasms) in the leech egg is a three-step segregation process. Int J Dev Biol 1998;42:149–162. [PubMed: 9551860]

Fernández J, Valladares M, Fuentes R, Ubilla A. Reorganization of cytoplasm in the zebrafish oocyte and egg during early steps of ooplasmic segregation. Dev Dyn 2006;235:656–671. [PubMed: 16425221]

Grant B, Hirsh D. Receptor-mediated endocytosis in the *Caenorhabditis elegans* oocyte. Mol Biol Cell 1999;10:4311–26. [PubMed: 10588660]

Gutzeit HO, Koppa R. Time-lapse film analysis of cytoplasmic streaming during late oogenesis of *Drosophila*. J Embryol Exp Morphol 1982;67:101–111.

Hackney DD, Stock MF. Kinesin's IAK tail domain inhibits initial microtubule-stimulated ADP release. Nat Cell Biol 2000;2:257–260. [PubMed: 10806475]

Harris JE, Govindan JA, Yamamoto I, Schwartz J, Kaverina I, Greenstein D. Major sperm protein signaling promotes oocyte microtubule reorganization prior to fertilization in *Caenorhabditis elegans*. Dev Biol 2006;299:105–121. [PubMed: 16919258]

Januschke J, Gervais L, Dass S, Kaltschmidt JA, Lopez-Schier H, St Johnston D, Brand AH, Roth S, Guichet A. Polar transport in the *Drosophila* oocyte requires Dynein and Kinesin I cooperation. Curr Biol 2002;12:1971–1981. [PubMed: 12477385]

Jeffery WR, Wilson LJ. Localization of messenger RNA in the cortex of *Chaetopterus* eggs and early embryos. J Embryol Exp Morphol 1983;75:225–39. [PubMed: 6684146]

Kamath RS, Fraser AG, Dong Y, Poulin G, Durbin R, Gotta M, Kanapin A, Le Bot N, Moreno S, Sohrmann M, et al. Systematic functional analysis of the *Caenorhabditis elegans* genome using RNAi. Nature 2003;421:231–237. [PubMed: 12529635]

Kim JK, Gabel HW, Kamath RS, Tewari M, Pasquinelli A, Rual JF, Kennedy S, Dybbs M, Bertin N, Kaplan JM, Vidal M, Ruvkun G. Functional genomic analysis of RNA interference in *C. elegans*. Science 2005;308:1164–1167. [PubMed: 15790806]

Kirby C, Kusch M, Kemphues K. Mutations in the *par* genes of *Caenorhabditis elegans* affect cytoplasmic reorganization during the first cell cycle. Dev Biol 1990;142:203–215. [PubMed: 2227096]

Kural C, Kim H, Syed S, Goshima G, Gelfand VI, Selvin PR. Kinesin and dynein move a peroxisome in vivo: tug of war or coordinated movement ? Science 2005;308:1469–1472. [PubMed: 15817813]

Leung CF, Webb SE, Miller AL. On the mechanism of ooplasmic segregation in single-cell zebrafish embryos. Dev Growth Differ 2000;42:29–40. [PubMed: 10831041]

Malone CJ, Misner L, Le Bot N, Tsai MC, Campbell JM, Ahringer J, White JG. The *C. elegans* hook protein, ZYG-12, mediates the essential attachment between the centrosome and nucleus. Cell 2003;115:825–836. [PubMed: 14697201]

Maruyama R, Velarde NV, Klancer R, Gordon S, Kadandale P, Parry JM, Hang JS, Rubin J, Stewart-Michaelis A, Schweinsberg P, Grant BD, Piano F, Sugimoto A, Singson A. EGG-3 regulates cell-surface and cortex rearrangements during egg activation in *Caenorhabditis elegans*. Curr Biol 2007;17:1555–1560. [PubMed: 17869112]

McCarter J, Bartlett B, Dang T, Schedl T. On the control of oocyte meiotic maturation and ovulation in *Caenorhabditis elegans*. Dev Biol 1999;205:111–128. [PubMed: 9882501]

McGee MD, Stagljar I, Starr DA. KDP-1 is a nuclear envelope KASH protein required for cell-cycle progression. J Cell Sci 2009;122:2895–2905. [PubMed: 19638405]

McNally K, Audhya A, Oegema K, McNally FJ. Katanin controls mitotic and meiotic spindle length. J Cell Biol 2006;175:881–891. [PubMed: 17178907]

McNally KL, McNally FJ. Fertilization initiates the transition from anaphase I to metaphase II during female meiosis in *C. elegans*. Dev Biol 2005;282:218–230. [PubMed: 15936342]

Mei W, Lee KW, Marlow FL, Miller AL, Mullins MC. hnRNP I is required to generate the Ca2+ signal that causes egg activation in zebrafish. Development 2009;136:3007–3017. [PubMed: 19666827]

Meyerzon M, Fridolfsson HN, Ly N, McNally FJ, Starr DA. UNC-83 is a nuclear-specific cargo adaptor for kinesin-1-mediated nuclear migration. Development 2009;136:2725–2733. [PubMed: 19605495]

Miller DM, Shakes DC. Immunofluorescence microscopy. Methods Cell Biol 1995;48:365–394. [PubMed: 8531735]

Pfeiffer DC, Gard DL. Microtubules in *Xenopus* oocytes are oriented with their minus-ends towards the cortex. Cell Motil Cyto 1999;44:34–43.

Pilling AD, Horiuchi D, Lively CM, Saxton WM. Kinesin-1 and Dynein are the primary motors for fast transport of mitochondria in *Drosophila* motor axons. Mol Biol Cell 2006;17:2057–2068. [PubMed: 16467387]

Poteryaev D, Fares H, Bowerman B, Spang A. *Caenorhabditis elegans* SAND-1 is essential for RAB-7 function in endosomal traffic. EMBO J 2007;26:301–312. [PubMed: 17203072]

Praitis V, Casey E, Collar D, Austin J. Creation of low-copy integrated transgenic lines in *Caenorhabditis elegans*. Genetics 2001;157:1217–1226. [PubMed: 11238406]

Robert VJ, Sijen T, van Wolfswinkel J, Plasterk RH. Chromatin and RNAi factors protect the C. elegans germline against repetitive sequences. Genes Dev 2005;19:782–787. [PubMed: 15774721]

Roosen-Runge EC. On the early development bipolar differentiation and cleavage of the zebrafish, *Brachydanio rerio*. Biol Bull 1938;75:119–133.

Sato M, Grant BD, Harada A, Sato K. Rab11 is required for synchronous secretion of chondroitin proteoglycans after fertilization in *Caenorhabditis elegans*. J Cell Sci 2008;121:3177–3186. [PubMed: 18765566]

Sato K, Sato M, Audhya A, Oegema K, Schweinsberg P, Grant BD. Dynamic regulation of caveolin-1 trafficking in the germ line and embryo of *Caenorhabditis elegans*. Mol Biol Cell 2006;17:3085–3094. [PubMed: 16672374]

Serbus LR, Cha BJ, Theurkauf WE, Saxton WM. Dynein and the actin cytoskeleton control kinesin-driven cytoplasmic streaming in *Drosophila* oocytes. Development 2005;132:3743–3752. [PubMed: 16077093]

Severson AF, Baillie DL, Bowerman B. A Formin Homology protein and a profilin are required for cytokinesis and Arp2/3-independent assembly of cortical microfilaments in *C. elegans*. Curr Biol 2002;12:2066–2075. [PubMed: 12498681]

Sheeman B, Carvalho P, Sagot I, Geiser J, Kho D, Hoyt MA, Pellman D. Determinants of *S. cerevisiae* dynein localization and activation: implications for the mechanism of spindle positioning. Curr Biol 2003;13:364–372. [PubMed: 12620184]

Timmons L, Court DL, Fire A. Ingestion of bacterially expressed dsRNAs can produce specific and potent genetic interference in *Caenorhabditis elegans*. Gene 2001;263:103–112. [PubMed: 11223248]

Vale RD, Schnapp BJ, Reese TS, Sheetz MP. Movement of organelles along filaments dissociated from the axoplasm of the squid giant axon. Cell 1985;40:449–454. [PubMed: 2578324]

van der Voet M, Berends CW, Perreault A, Nguyen-Ngoc T, Gönczy P, Vidal M, Boxem M, van den Heuvel S. NuMA-related LIN-5, ASPM-1, calmodulin and dynein promote meiotic spindle rotation independently of cortical LIN-5/GPR/Galpha. Nat Cell Biol 2009;11:269–277. [PubMed: 19219036]

Yang HY, Mains PE, McNally FJ. Kinesin-1 mediates translocation of the meiotic spindle to the oocyte cortex through KCA-1, a novel cargo adapter. J Cell Biol 2005;169:447–457. [PubMed: 15883196]

Yang HY, McNally K, McNally FJ. MEI-1/katanin is required for translocation of the meiosis I spindle to the oocyte cortex in *C elegans*. Dev Biol 2003;260:245–259. [PubMed: 12885567]

Zhou K, Rolls MM, Hall DH, Malone CJ, Hanna-Rose W. A ZYG-12-dynein interaction at the nuclear envelope defines cytoskeletal architecture in the *C. elegans* gonad. J Cell Biol 2009;186:229–241. [PubMed: 19635841]

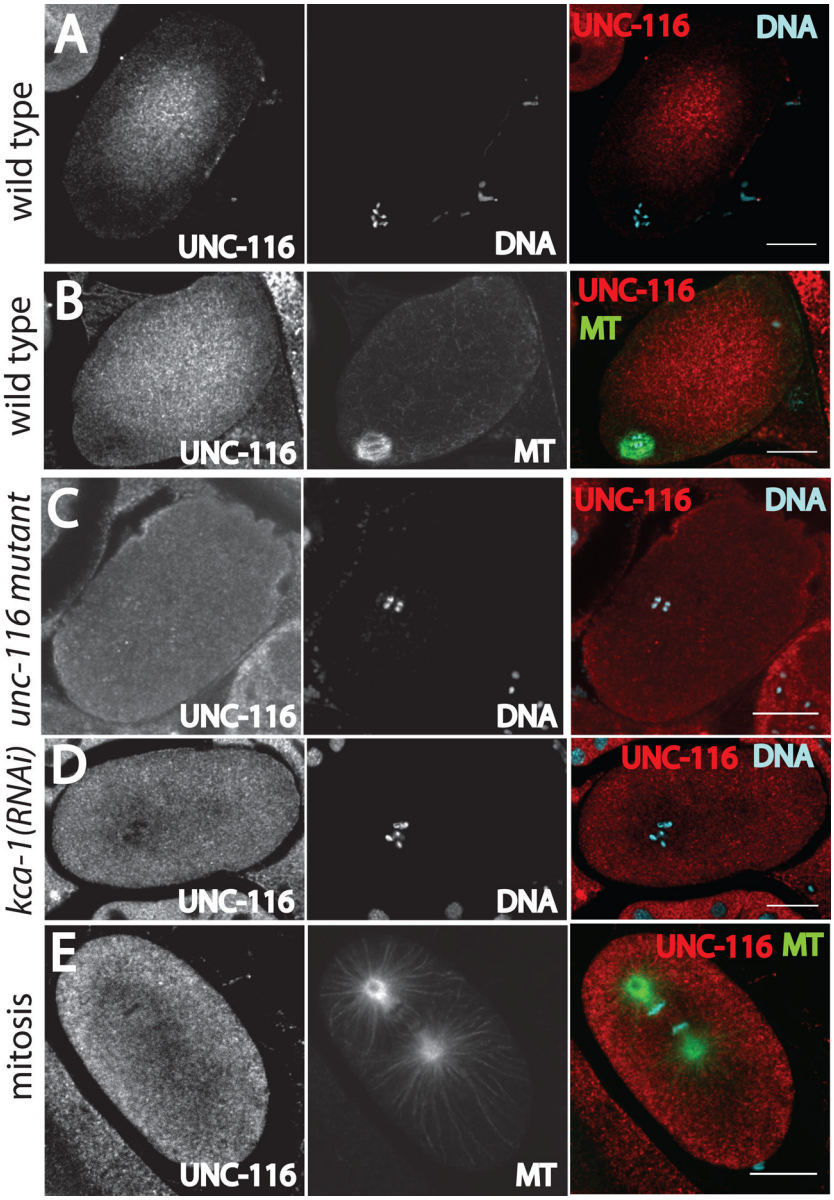

Figure 1. Antibody labeling of fixed embryos reveals that the kinesin-1 heavy chain, UNC-116, is concentrated in the cytoplasm in the middle of meiotic embryos

A and B. Wild-type meiotic embryos, C. meiotic embryo of *unc-116* mutant with reduced levels of UNC-116 protein (see Methods and Fig. S1), D. meiotic embryo from *kca-1(RNAi)* worm, and E. wild-type mitotic embryo. MT indicates microtubules labeled with an anti-α tubulin antibody. DNA indicates staining with DAPI. The images in the right column are merged images. All images were acquired with a laser scanning confocal microscope. Bars = 10 μm.

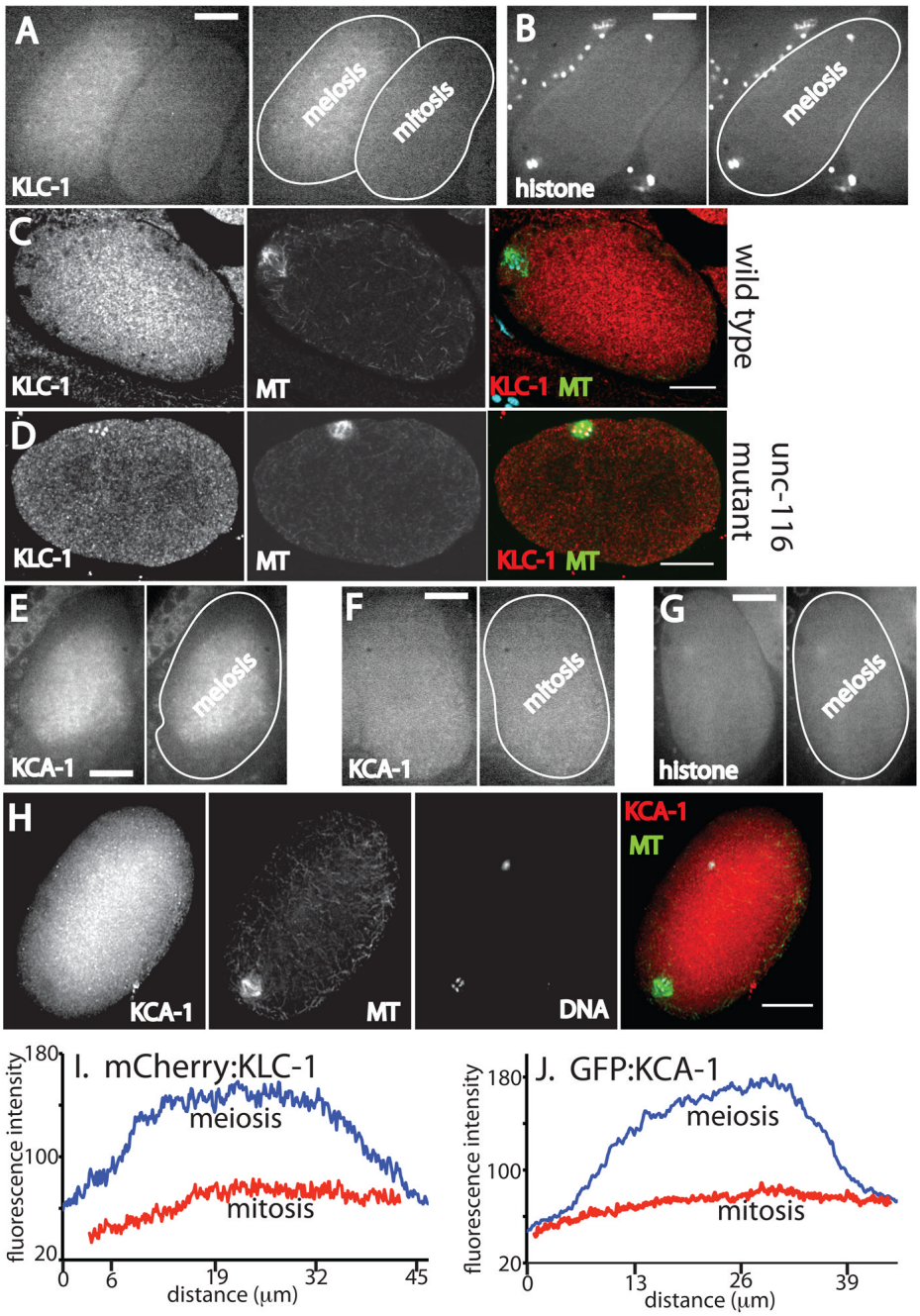

Figure 2. KLC-1 and KCA-1 are concentrated in the middle of meiotic embryos

A. Spinning disk confocal image of mCherry:KLC-1 fluorescence in living embryos *in utero*. A meiotic embryo is on the left and a one-celled mitotic embryo is on the right. In the right panel, the outlines of the embryos have been highlighted for clarity. B. Spinning disk confocal image of mCherry:histone H2b cytoplasmic fluorescence in a living meiotic embryo *in utero*. C and D. Laser scanning confocal images of anti-KLC-1 antibody staining in fixed meiotic embryos, C is wild type, D is an *unc-116* mutant (FM78). E. Spinning disk confocal image of GFP:KCA-1 fluorescence in a living meiotic embryo in *utero*. F. Spinning disk confocal image of GFP:KCA-1 fluorescence in a living mitotic embryo *in utero*. G. Spinning disk confocal image of GFP:histone H2b cytoplasmic fluorescence in a living meiotic embryo

in utero. The chromosomes are not in this focal plane. H. Deconvolved widefield image of anti-KCA-1 staining of a fixed meiotic embryo. MT indicates microtubules labeled with an anti-α tubulin antibody. DNA indicates staining with DAPI. The color images are merged images. Size bars = 10 μm. I and J. Fluorescence intensity line scans across the long axis of a meiotic embryo and a mitotic embryo expressing mCherry-KLC-1 (I) or GFP:KCA-1 (J).

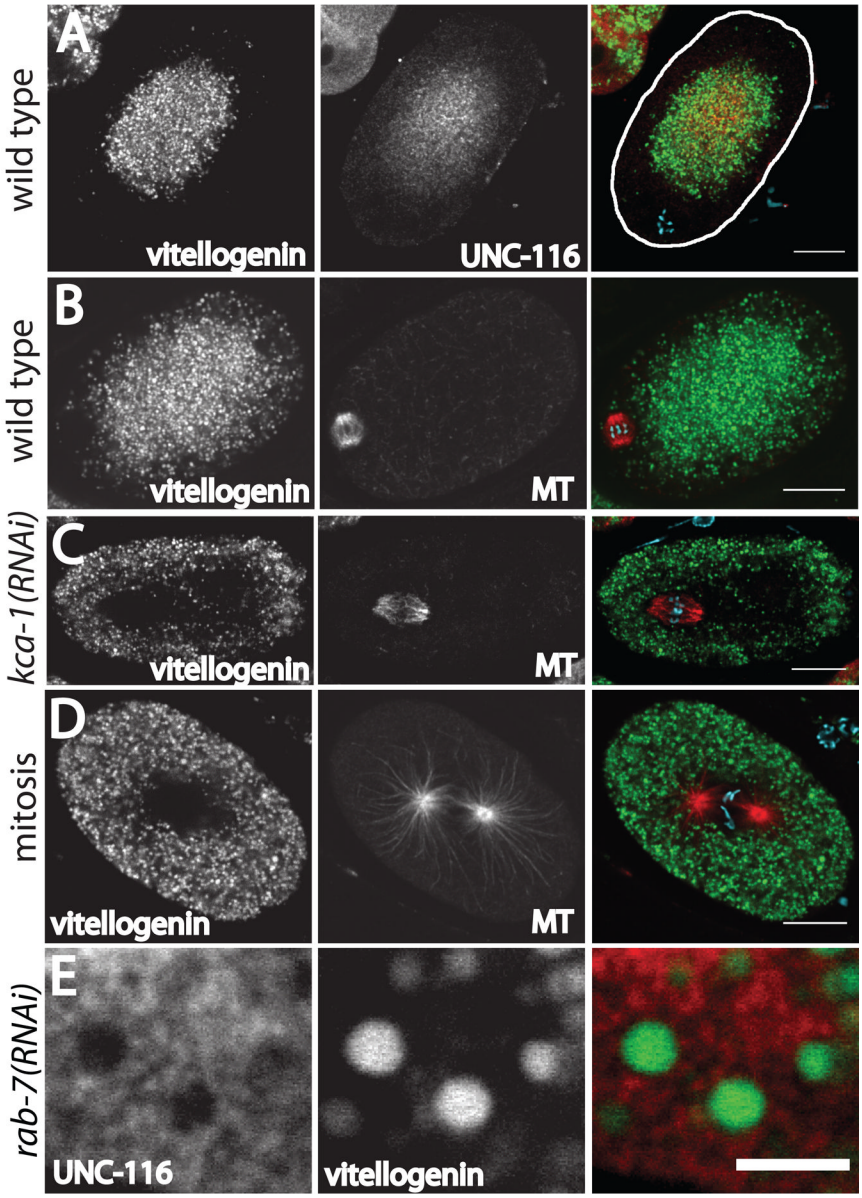

Figure 3. Yolk granules are concentrated in the middle of meiotic embryos in a KCA-1-dependent manner

Laser scanning confocal images of GFP:vitellogenin fluorescence in fixed embryos. A. UNC-116 is concentrated in the same region of a wild-type meiotic embryo as the yolk granules. The cortex is highlighted for clarity on the right. B. The spindle is in a yolk granule-free area near the cortex in a wild-type meiotic embryo. C. In a *kca-1(RNAi)* meiotic embryo, the relative positions of the spindle and yolk granules are inverted. D. Yolk granules extend all the way to the cortex in a wild-type mitotic embryo. MT indicates microtubules labeled with an anti-α tubulin antibody. The color images are merged images in which blue indicates chromosomes stained with DAPI. Bar in A–D = 10 μm. E. In a *rab-7(RNAi)* meiotic embryo, vitellogenin is trapped in endosomal intermediates that are much larger than wild-type yolk granules (Poteryaev et al., 2007). UNC-116 is not discernibly concentrated on the surface of these vesicles. Bar in E = 3 μm.

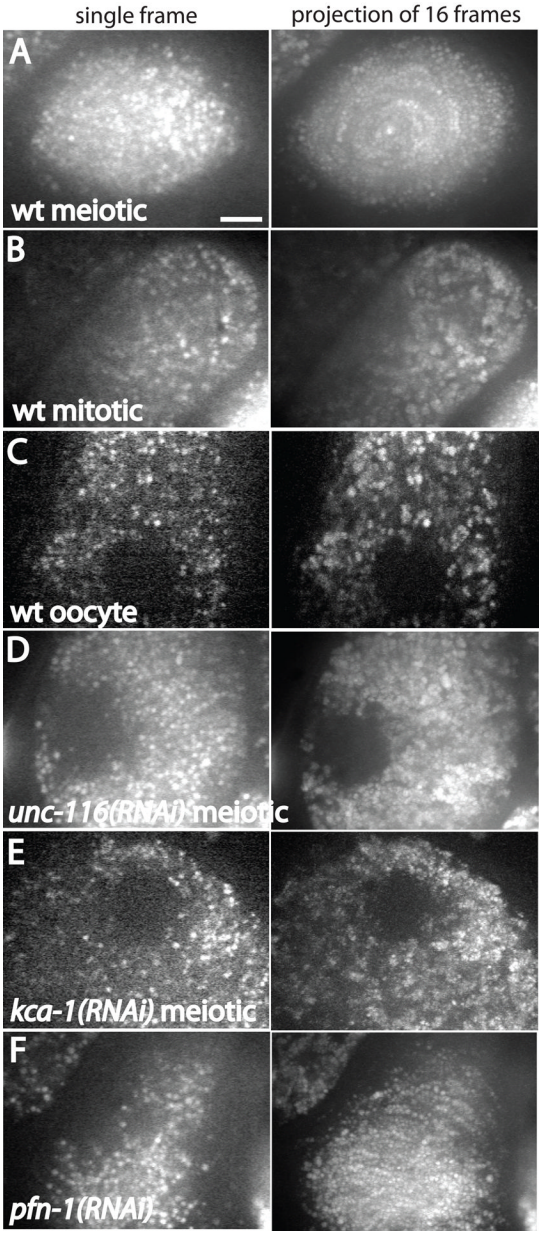

Figure 4. Projections of time-lapse images of GFP:vitellogenin-containing yolk granules reveal kinesin-dependent circular movement in meiotic embryos

Single 300 ms exposures are shown on the left. Images on the right are maximum intensity projections of 16 frames captured at 4 sec intervals. A. In a wild-type meiotic embryo, a circular pattern is generated in the time series projection. B. a wild-type mitotic embryo, C. a wild-type diakinesis oocyte, D. an *unc-116(RNAi)* meiotic embryo, E. or a *kca-1(RNAi)* meiotic embryo, no circular movements are seen. Instead, yolk granules appear larger in the time series projection due to Brownian motion. F. In profilin-depleted meiotic embryos, long curved arcs appeared in projections due to circular movements of yolk granules. Profilin is required for assembly of all actin structures in the one-celled embryo (Severson et al., 2002) and the uterus of this worm contained only one-celled, multi-nucleate embryos, indicating that the RNAi was penetrant. Bar = 5 μm.

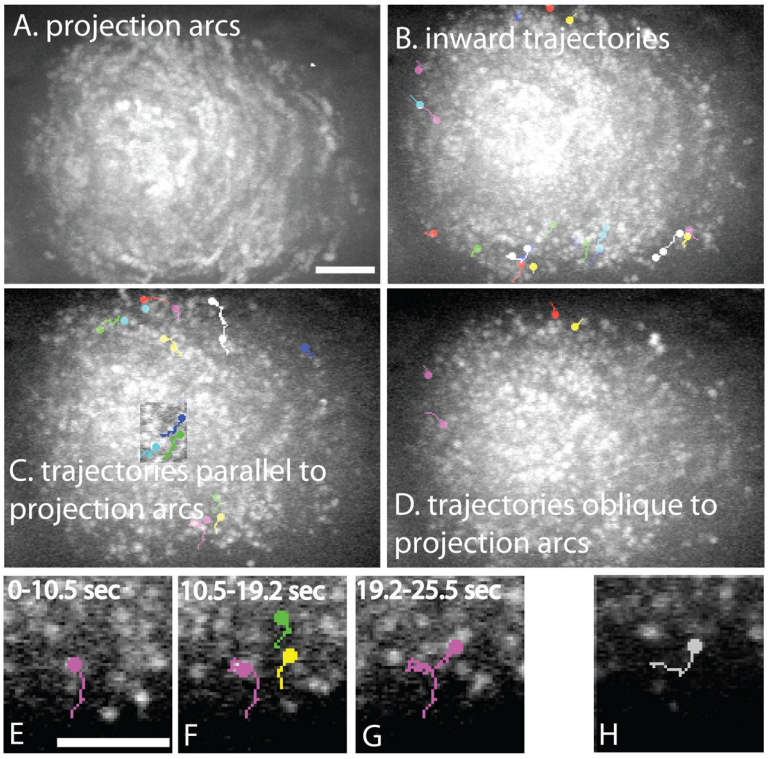

Figure 5. Single particle tracking reveals inward movement of yolk granules from the cortex

Images of GFP:vitellogenin fluorescence in a wild-type meiotic embryo were captured at 300 ms intervals using a spinning disk confocal microscope. A. Maximum intensity projection of a time-series reveals arcs indicative of net circular movement. B. Single particle tracks moving diagonally inward. The circles indicate the end of each track. A maximum intensity projection is shown so that movements occurring at different times during a 60 sec period can be shown in a single image. C. Examples of single particle tracks that parallel the projection arcs shown in A and follow paths parallel to the cortex. Note that single particle tracks are shorter and straighter than the projection arcs. The square in the middle of the embryo is an overlay of a projection of a smaller time series because the particle tracks within this square were completely obscured in the full time-series projection. D. Examples of single particle tracks that are perpendicular to the projection arcs. E. Magnified region showing the pink track of a yolk granule moving on a linear track for 10.5 sec. F. From 10.5–19.2 sec, the yolk granule with the pink track underwent Brownian motion with no net displacement while 2 other yolk granules (green and yellow tracks) moved on parallel linear tracks. G. After the yolk granules with green and yellow tracks exited the focal plane, the pink-track yolk granule resumed linear motion. H. Example of a single particle track showing a yolk granule making a 90° turn. Bars = 5 μm. Bar in A is for A, B, C and D. Bar in E is for E, F, G and H.

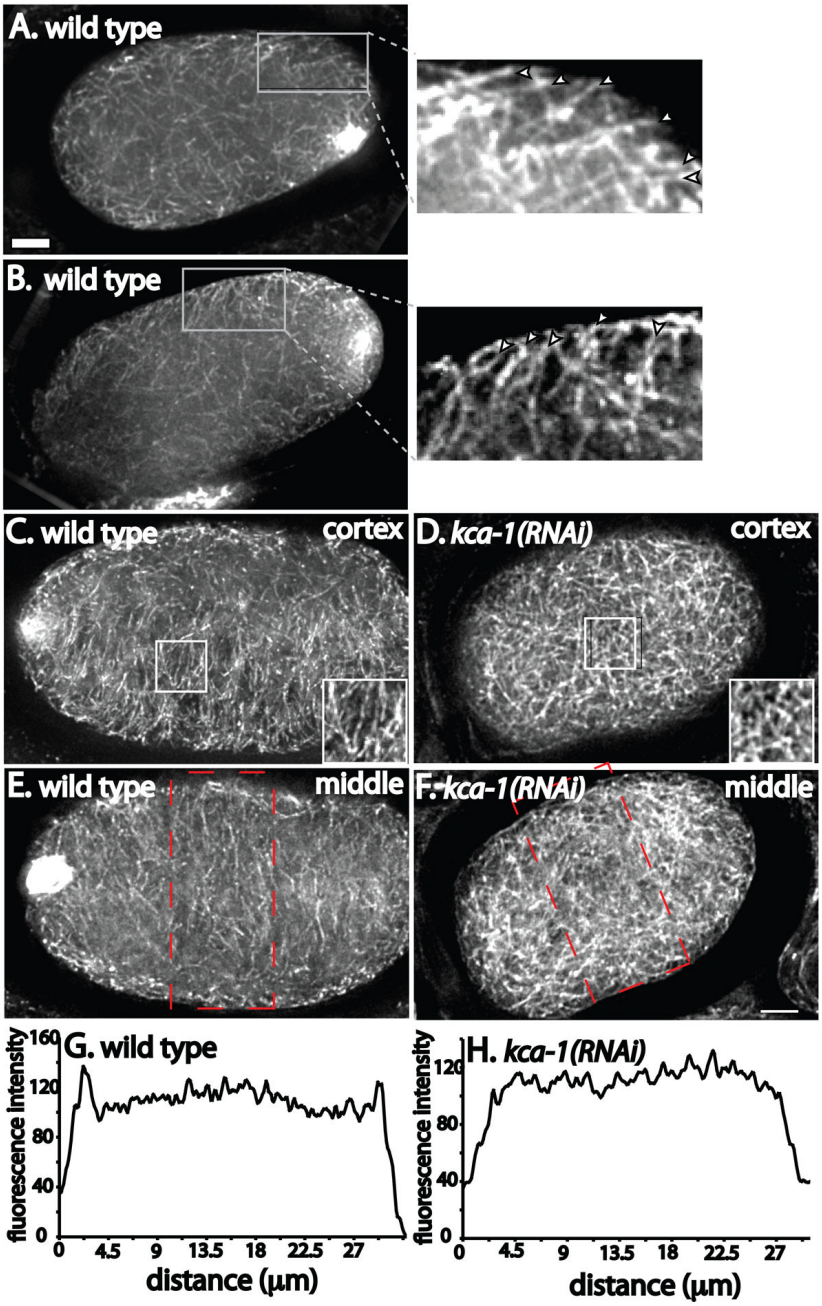

Figure 6. Parallel cytoplasmic microtubules extend diagonally inward from the cortex of meiotic embryos

Meiotic embryos were fixed and stained with anti-α tubulin antibody. Images were captured every 200 nm in the z axis and deconvolved. A is a projection of 22 images (4.4 μm thick), B–F are projections of 10 images (2 μm thick). A and B. Examples of wild-type meiotic embryos with insets showing higher magnification of parallel microtubules extending diagonally inward from the cortex. C and D show surface views of cortical microtubules showing parallel microtubules in the wild-type embryo in C and randomly oriented microtubules in the *kca-1 (RNAi)* embryo in D. E and F show a focal plane in the middle of the embryo showing a higher density of microtubules at the cortex in the wild-type embryo (E) and a more even distribution

of microtubules in the *kca-1(RNAi)* embryo (F). G and H show fluorescence intensity plots across the width of the embryos (indicated by the red boxes) in E and F. Bar = 5 μm.

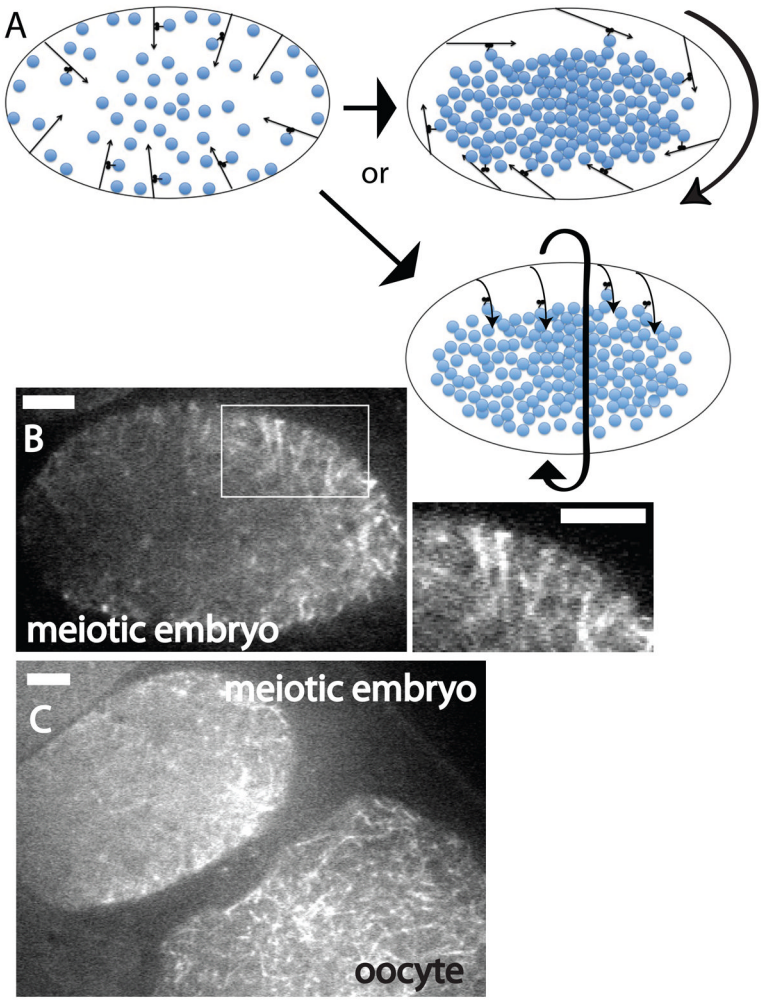

Figure 7. Cytoplasmic microtubules in living wild-type meiotic meiotic embryos

A. Model in which yolk granules (blue circles) are initially transported by kinesin-1 inward on microtubules with minus ends anchored in the cortex. Thin arrows represent cytoplasmic microtubules (arrowhead = plus end). Curved, thick arrows represent the direction of streaming. As yolk granules increase in number due to endocytosis of vitellogenin, the middle of the embryo becomes completely packed with yolk granules and the plus ends of cortically anchored microtubules are forced to pivot outward. This outward pivoting increases the density of microtubules at the cortex and initiates circular cytoplasmic streaming. When microtubules pivot down the long axis of the embryo (upper right), streaming occurs down the long axis of the embryo (Video 1). When microtubules pivot in the short axis of the embryo, lower right, streaming initiates down the short axis of the embryo (Video 2). B and C. Spinning disk confocal images of GFP:tubulin fluorescence in living wild-type meiotic embryos. B. Parallel microtubules extend diagonally inward from the cortex in the apparent direction of streaming. A magnified view of the area within the white rectangle is shown on the right. C. Microtubules are barely discernible in the meiotic embryo (upper left) but are clearly discernible in the diakinesis oocyte (lower right) most likely because most of the microtubules in meiotic embryos move during the 1.5 sec exposure required to capture these images whereas microtubules in diakinesis oocytes are mostly stationary. Bar = 5μm.

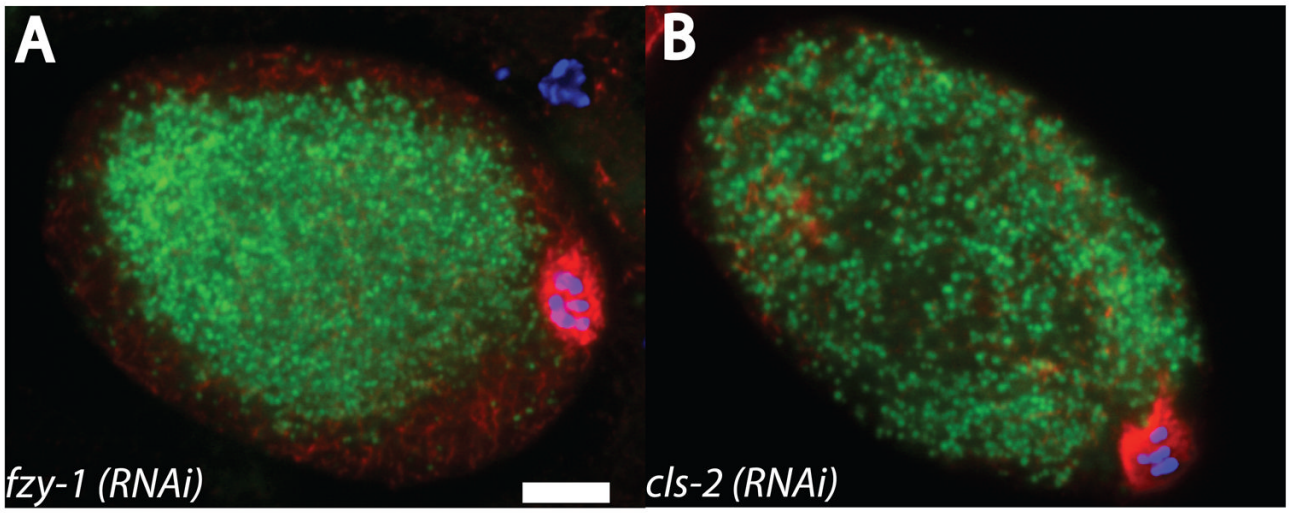

Figure 8. Yolk granules are dispersed but spindle translocation is normal in *cls-2(RNAi)* meiotic embryos

Metaphase I meiotic embryos expressing GFP:vitellogenin (green) were fixed and stained with anti-tubulin antibody (red) and DAPI (blue). A. *fzy-1* (RNAi) embryo. B. *cls-2(RNAi)* embryo. Bar = 5 μm.

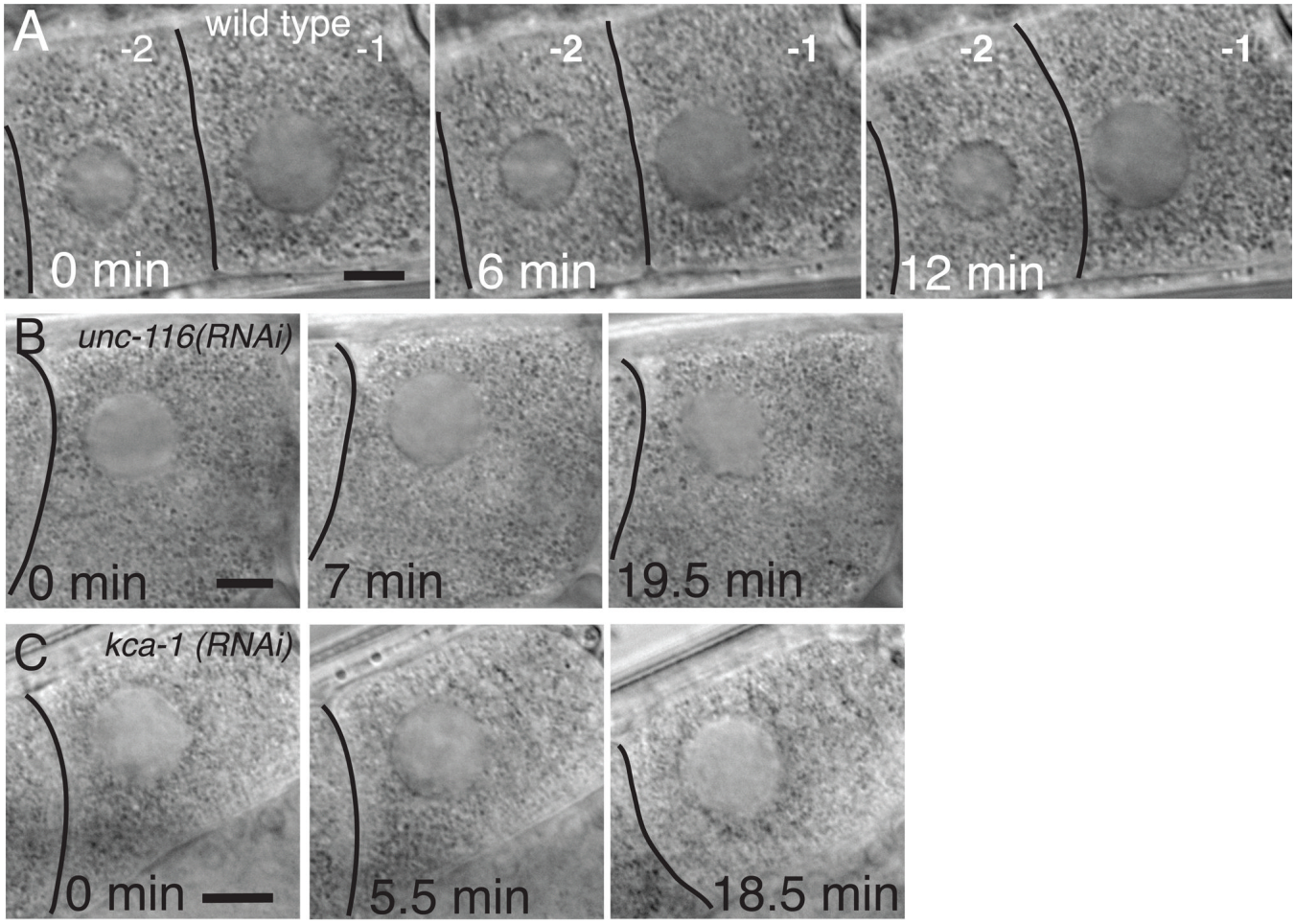

Figure 9. Kinesin-1 is required for migration of the diakinesis nucleus toward the oocyte cortex

A. Brightfield images from a time-lapse series of the -1 oocyte in a wild-type worm showing migration of the nucleus toward the junction between the -1 and -2 oocyte. The nucleus is centered within the -2 oocyte. Two discrete processes result in the asymmetric position of the nucleus in the -1 oocyte at nuclear envelope breakdown. The distance between the nucleus and the junction with the -2 oocyte decreases, indicating nuclear migration, and the oocyte changes shape such that it extends asymmetrically toward the spermatheca, which is to the right in these images. Nuclear migration occurred in 17/18 wild-type worms in which germinal vesicle breakdown and ovulation occurred. In 6/6 *unc-116(RNAi)* worms (B) and 5/5 *kca-1(RNAi)* worms (C) in which germinal vesicle breakdown occurred, no nuclear migration took place but the oocyte still extended asymmetrically toward the spermatheca. Bar = 7 μm.

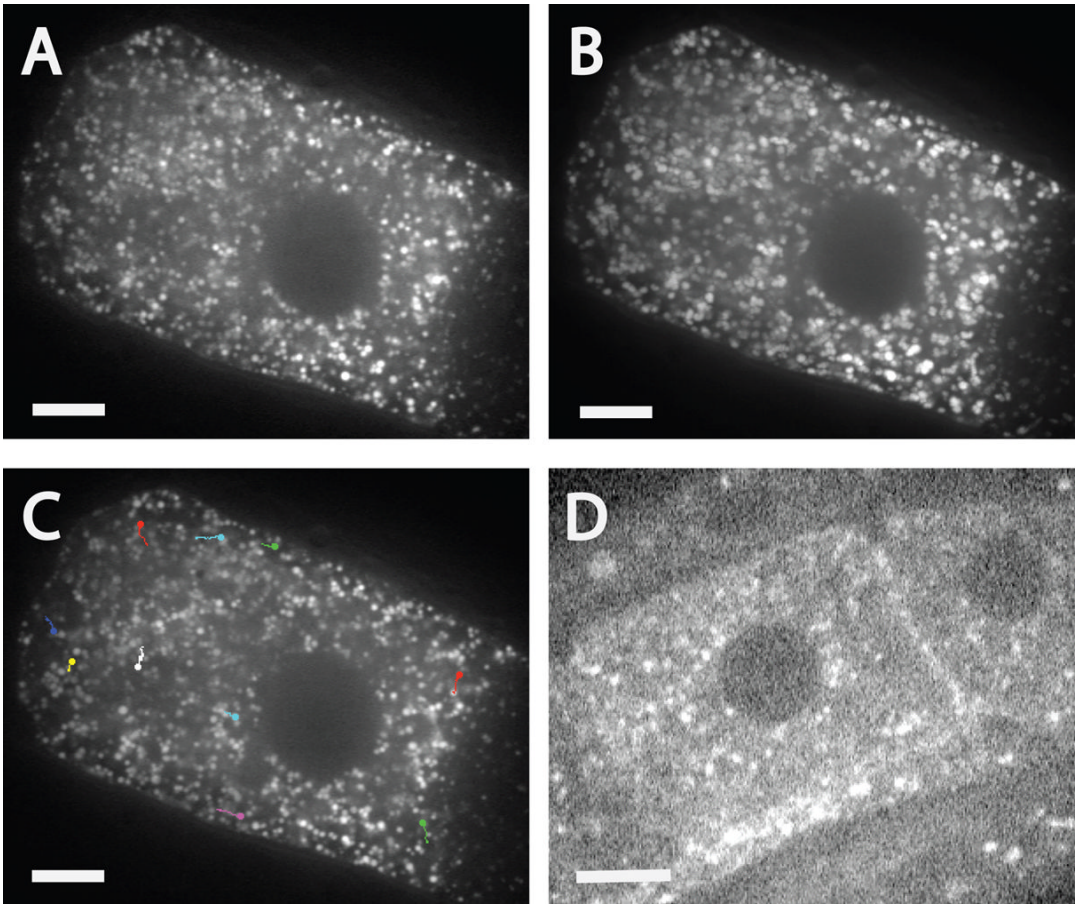

Figure 10. Yolk granule transport is suppressed in diakinesis oocytes relative to meiotic embryos

A and B. Comparison of a single time point image of GFP:vitellogenin-labeled yolk granules in a diakinesis oocyte (A) with a maximum intensity projection of a 10 sec time series (B) reveals that most yolk granules are stationary. C. Tracks show the infrequent, short, linear movements of a small fraction of the yolk granules in a diakinesis oocyte. D. Confocal image of mCherry:KCA-1 fluorescence in a diakinesis oocyte. Fluorescence is concentrated in discrete foci that are not observed in meiotic embryos. Bar = 7 μm.

Table 1

Depletion of kinesin-1 subunits results in diakinesis nuclei that are further from the cortex at nuclear envelope breakdown

Measurements were taken from time-lapse sequences of GFP:tubulin fluorescence or GFP:histone fluorescence

genotype	Distance from cortex (μm)	Standard Deviation (μm)	n
Wild type	1.32	.47	17
unc-116(RNAi)	8.43	1.67	14
klc-1(RNAi)	5.50	2.11	9
kca-1(RNAi)	6.56	2.18	25